IIETA International Information and Engineering Technology Association
Advancing the World of Information and Engineering

Journal Européen des Systèmes Automatisés
Vol. 59, No. 10, October, 2026, pp. 2949-2965
Journal homepage: http://iieta.org/journals/jesa

Adaptive Cluster Sizing and a Reliability-Aware Multi-Hop Backbone for Automated Data Aggregation in Wireless Sensor Networks: A Link-Consistent Evaluation with Component-Level Attribution

Ammar Alauldeen Abdulmajeed*, Omar Ibrahim Mustafa Al-Azzawi, Mohanad Mezher

Department of Computer Engineering Techniques, Electrical Engineering Technical College, Middle Technical University, Baghdad 10001, Iraq

Corresponding Author Email: ammar@mtu.edu.iq

Copyright: ©2026 The authors. This article is published by IIETA and is licensed under the CC BY 4.0 license (http://creativecommons.org/licenses/by/4.0/).

https://doi.org/10.18280/jesa.591016

Received: 11 August 2026
Revised: 20 October 2026
Accepted: 27 October 2026
Available online: 31 October 2026

Keywords:
ablation study, adaptive cluster count, automated network operation, data aggregation, energy efficiency, link reliability, multi-hop backbone routing, wireless sensor networks

ABSTRACT

Fuzzy-metaheuristic clustering dominates data aggregation design in wireless sensor networks (WSNs), yet its gains are rarely attributed to specific components and are usually measured on idealised links. This paper presents UA-IT2F/AEO, a multi-scale aggregation framework whose core is an analytically adaptive cluster count and an energy- and reliability-aware multi-hop backbone re-optimised every round; an interval type-2 fuzzy aggregator score and an uncertainty-aware adaptive Equilibrium Optimizer (EO) are added as hypotheses to be tested. The framework is evaluated under log-normal shadowing with truncated automatic repeat request (ARQ), in which every retransmission costs energy, across three scenarios with twenty deployments each, paired significance tests and effect sizes. Relative to the strongest baseline, it raises the packet delivery ratio (PDR) to 0.874-0.989 and reduces energy per delivered bit by 21.1-22.1% (Holm-corrected $p < 2 \times 10^{-4}$). A component-level ablation shows that these gains come almost entirely from the adaptive cluster count and the multi-hop backbone, whereas the type-2 layer and the adaptive controller have no significant network-level effect. The control messages required are estimated to cost 0.6-2.3% of the data energy. The results identify feedback-driven structural scheduling as the main lever for automated WSN operation and caution against crediting components that have not been isolated.

1. INTRODUCTION

Wireless sensor networks (WSNs) underpin environmental monitoring, industrial automation and clinical telemetry, and in all of these settings the dominant energy cost is radio communication rather than sensing or computation. In-network data aggregation, in which intermediate nodes combine correlated readings before forwarding them, is therefore the principal lever available to a protocol designer. The canonical clustering protocols - Low-Energy Adaptive Clustering Hierarchy (LEACH) [1, 2], Power-Efficient Gathering in Sensor Information Systems (PEGASIS) [3] and Hybrid Energy-Efficient Distributed clustering (HEED) [4] - established the architecture that almost all later work inherits: elect cluster heads (CHs), attach members to them, aggregate locally, and forward towards a sink. Because CH election is a combinatorial decision under multiple competing criteria, the field has converged on a design pattern that couples a fuzzy inference system, which scores candidate nodes from residual energy, distance, and link quality, with a population-based metaheuristic that searches the space of CH assignments [5-7]. Recent instances of this pattern report large improvements over LEACH and its fuzzy variants. A representative and recent example is the Fuzzy-Controlled Equilibrium Optimizer (FCEO) of Idan et al. [8], which combines a 27-rule Mamdani system [9, 10] with the Equilibrium Optimizer (EO) [11] over a three-level node-CH-gateway-sink hierarchy.

Two methodological weaknesses are, however, nearly universal in this literature, and they interact badly. The first concerns the channel. Most evaluations assume that a transmission succeeds whenever it is attempted, so packet delivery ratio (PDR) becomes an artefact of node death rather than a property of the links, and the energy wasted on retransmissions - the very quantity that a reliability-aware protocol is supposed to save - is absent from the energy model. The second concerns attribution. A new protocol typically bundles four or five mechanisms and is compared only against external baselines, so the aggregate improvement is tacitly credited to the headline intelligent component. Whether the fuzzy layer or the metaheuristic actually carries that improvement is rarely tested. This is precisely the criticism that has been levelled at metaphor-driven optimisation more broadly [12-14].

These weaknesses also matter outside the protocol literature. In an industrial monitoring network, CH election and routing form the actuation layer of an automated control loop: the network measures its own state (residual energy and link quality), a supervisory optimizer turns those measurements into a schedule of CHs and forwarding parents, and the resulting traffic changes the state that is measured next

[15]. Designing such a loop requires knowing which of its elements actually regulates the controlled quantities - here, energy per delivered bit and delivery ratio - and how often each must be updated. A component that adds computation and configuration effort without a measurable effect on the closed loop is a cost to the operator rather than a feature.

This paper addresses both weaknesses. We propose UA-IT2F/AEO (uncertainty-aware interval type-2 fuzzy/adaptive Equilibrium Optimizer), a multi-scale aggregation framework whose core is structural: an analytically adaptive cluster count and an energy- and reliability-aware multi-hop backbone that is re-optimised on a faster time scale than clustering. Around this core it places an interval type-2 (IT2) fuzzy decision module and an uncertainty-aware adaptive EO, which we treat as hypotheses rather than as established sources of gain. We evaluate the framework under an explicit link model with retransmission accounting, and we then dismantle it component by component to establish where its advantage actually originates. The name UA-IT2F/AEO is retained for the complete configuration so that every component can be referred to consistently. The specific contributions are:

(1) A link-consistent evaluation model. Frame delivery is derived from a log-normal shadowing path-loss model with temporally correlated fading, and each hop uses truncated automatic repeat request (ARQ) in which every attempt, successful or not, is charged to both transmitter and receiver. Aggregation gain is tied to intra-cluster spatial correlation [16] rather than assumed constant.

(2) A multi-scale, feedback-driven architecture, which is *the main technical contribution.* Clustering is solved on a slow time scale while the inter-CH backbone is re-solved every round from current residual energy and link statistics, which lets the sink-adjacent relay rotate before it is drained. The cluster count is adapted from an analytic optimum corrected for the fact that the backbone is multi-hop. Section 6.7 shows that these two mechanisms carry almost all of the measured improvement.

(3) An uncertainty-aware decision and search layer, examined as a hypothesis. An interval type-2 fuzzy system [17-20] scores candidate aggregators, with a footprint of uncertainty (FOU) that is not a fixed design constant but is driven at run time by the observed volatility and scarcity of each node's link-quality estimate. Its interval width is exported as an uncertainty index that modulates the exploration of an adaptive EO. Section 4.2 gives a physical interpretation and a numerical example of this mechanism, and Section 6.7 tests whether it matters.

(4) A component-level attribution study with sensitivity and cost checks. Eight ablated variants, including one in which CH election is replaced by uniform random selection, are compared against the full model with paired tests. The result is partly negative and is reported as such: the type-2 layer and the adaptive optimizer controller do not produce statistically significant network-level gains, while the adaptive cluster count and the multi-hop backbone do. A sensitivity check on the fitness weights and an analytical estimate of the control-message overhead (Sections 6.8 and 6.9) bound how far these conclusions depend on design choices and on the cost of disseminating routing updates.

Section 2 reviews related work and the evidentiary standards it applies. Section 3 defines the system model. Section 4 develops the proposed framework. Section 5 states the experimental methodology, Section 6 reports results, Section 7 discusses them, including their role in automated network operation, Section 8 states threats to validity and Section 9 concludes.

2. RELATED WORK

2.1 Clustering and fuzzy cluster-head election

LEACH [1, 2] rotates CHs probabilistically to spread the head burden, but its election ignores residual energy and its single-hop CH-to-sink link is expensive in large fields. HEED [4] adds residual energy and communication cost to the election; PEGASIS [3] replaces clusters with a chain. Fuzzy election was introduced to combine incommensurable criteria without hand-tuned thresholds: Gupta et al. [6] score candidates from energy, concentration and centrality, and later fuzzy unequal-clustering schemes [7] size clusters to counter the sink-adjacent hot spot. Recent surveys classify this design space and its persistent open problems in detail [21, 22]. These remain the structural reference points for the present work.

2.2 Metaheuristic and learning-based aggregation

Swarm and physics-inspired optimizers have been applied extensively to CH selection and aggregation-tree construction [5], and recent hybrid and multi-objective variants continue that line [23-25]. The EO [11], inspired by control-volume mass balance, maintains an equilibrium pool that mixes exploration with exploitation and has been refined in several variants [26, 27]. Within WSN aggregation specifically, reported approaches include secure hybrid star-tree aggregation [28], perceptually-important-point data reduction [29], the CHESDA privacy-preserving scheme [30], geographical aggregation with mobile sinks [31], ant-colony path selection [32], hybrid spatio-temporal clustering [33], dragonfly-based secure aggregation trees [34], Q-learning aggregation-aware routing [35], the FAJIT fuzzy tree-formation scheme [36] and hybrid particle swarm optimisation (PSO) clustering [37]. FCEO [8] is the closest antecedent to this work and is reproduced here as a baseline. Across this body of work the reported limitations are consistent - premature convergence, weak adaptation to topology change, centralised bottlenecks - but the evidence standards vary widely. Table 1 summarises representative schemes along the dimensions that determine whether a reported gain can be trusted: whether frame loss is modelled at all, whether retransmission energy is charged, how many independent runs are reported, whether significance testing is performed, and whether the contribution of individual components is isolated. Because papers report their experimental assumptions in different ways, Table 1 distinguishes a feature that was explicitly excluded from one that was simply not reported. An entry is coded No only when the original paper states an idealised assumption, for example an energy model containing only the first-order radio terms with no channel error model, and n/r when the paper neither describes the feature nor states its absence. Schemes evaluated in packet-level simulators such as NS-2 or OMNeT++ may lose frames through the simulator's default physical and medium access control (MAC) layers even when this is not described; such cases are coded n/r rather than No, because the loss mechanism and its energy accounting cannot be determined from the paper. Coding a feature as n/r is therefore a statement about what the paper reports, not a judgement that the authors ignored it.

Table 1. Representative data aggregation schemes and the evidence reported in their evaluation

Ref.	Year	Scheme	Core Mechanism	Frame Loss Modelled	Retx Energy	Runs	Sig. Test	Ablation
[28]	2021	SHSDA	star-tree, light encryption	n/r	n/r	n/r	n/r	n/r
[29]	2022	PIP-DA	perceptual point reduction	n/r	n/r	n/r	n/r	n/r
[30]	2021	CHESDA	fuzzy + slice mixing	n/r	n/r	n/r	n/r	n/r
[31]	2025	GEADAMS	mobile sink rendezvous	n/r	n/r	n/r	n/r	n/r
[32]	2025	ACO agents	ant colony path selection	n/r	n/r	n/r	n/r	n/r
[34]	2021	Fuzzy+DA	dragonfly aggregation tree	n/r	n/r	n/r	n/r	n/r
[35]	2021	Q-routing	reinforcement learning	n/r	n/r	n/r	n/r	n/r
[36]	2021	FAJIT	fuzzy parent selection	n/r	n/r	n/r	n/r	n/r
[37]	2023	HPSO	hybrid PSO clustering	n/r	n/r	n/r	n/r	n/r
[8]	2026	FCEO	type-1 fuzzy + EO, gateways	No	No	10	n/r	n/r
This work	2026	UA-IT2F/AEO	type-2 fuzzy + adaptive EO + backbone	Yes	Yes	20	Yes	Yes

Note: Yes = modelled and described; No = excluded by an idealised assumption stated in the paper; n/r = not reported, i.e., the paper neither describes the feature nor states its absence. Retx = retransmission; Sig. = significance; ACO = ant colony optimisation; DA = dragonfly algorithm; PSO = particle swarm optimisation; EO = Equilibrium Optimizer.

2.3 The evaluation gap

Two observations follow from Table 1, subject to the distinction it draws between what was excluded and what was not reported. First, most schemes that claim reliability improvements do not report the mechanism by which frames are lost, so it cannot be established whether their PDR differences reflect link behaviour or merely differences in how long nodes survive. Second, none of the surveyed schemes reports an ablation that isolates its fuzzy or metaheuristic component against an otherwise identical architecture. The present work is designed to close both gaps, at the cost of reporting a result that is unfavourable to part of its own design.

3. SYSTEM MODEL AND PROBLEM FORMULATION

3.1 Network model and assumptions

N sensor nodes are deployed uniformly at random over a rectangular field of dimensions M × M, with a sink at a fixed known position that may lie inside or outside the field. Nodes are homogeneous in initial energy E_0, radio hardware and sensing range, are static, and know their own positions. Every alive node generates one k-bit reading per round. The sink is not energy constrained. Network dynamics arise from progressive battery depletion and from time-varying link quality, not from mobility; as nodes die, the surviving topology changes and both clustering and routing must adapt.

3.2 Radio energy model

The first-order radio model [1] is used, with the free-space and multipath components separated at the crossover distance d_0:

$$E_{tx}(k,d) = \begin{cases} E_{elec}k + \varepsilon_{fs}kd^2, & d < d_0 \\ E_{elec}k + \varepsilon_{mp}kd^4, & d \geq d_0 \end{cases} \quad (1)$$

$$d_0 = \sqrt{\varepsilon_{fs}/\varepsilon_{mp}} \quad (2)$$

Reception and aggregation are charged as in Eq. (3), where m is the number of packets combined and E_{DA} is the per-bit aggregation cost:

$$E_{rx}(k) = E_{elec}k, \qquad E_{da}(k,m) = E_{DA}\,k\,m \quad (3)$$

3.3 Link model and retransmission accounting

Unlike the evaluations surveyed in Table 1, frame delivery here is derived from the channel. Path loss follows a log-normal shadowing model [38]; estimating such links at run time is an active topic in its own right [39, 40]:

$$PL(d) = PL_0 + 10\,n\log_{10}\left(d/d_{ref}\right) + X, \qquad X \sim \mathcal{N}(0,\sigma^2) \quad (4)$$

Shadowing is not redrawn independently each round, because that would let a protocol average away fades that in reality persist. A per-node shadowing state evolves as a first-order autoregressive (AR(1)) process and link shadowing is formed from the two endpoint states, which preserves the marginal variance while inducing spatial and temporal correlation at O(N) cost per round:

$$s_i(r) = \rho\, s_i(r-1) + \sqrt{1-\rho^2}\;\xi_i(r) \quad (5)$$

$$X_{ij}(r) = \frac{s_i(r) + s_j(r)}{\sqrt{2}}, \qquad \gamma_{ij} = P_t - PL\left(d_{ij}\right) - P_n \quad (6)$$

The resulting signal-to-noise ratio yields a bit error rate (BER) and, for a k-bit frame, a packet reception ratio (PRR):

$$BER_{ij} = \frac{1}{2}\,\mathrm{erfc}\left(\sqrt{\gamma_{ij}^{lin}}\right), \qquad \pi_{ij} = \left(1 - BER_{ij}\right)^k \quad (7)$$

Each hop uses truncated automatic repeat request with at most R attempts. Both the success probability and the expected number of transmissions follow from the truncated geometric distribution:

$$P_{ij}^{s} = 1 - \left(1-\pi_{ij}\right)^R, \qquad \mathbb{E}\left[T_{ij}\right] = \frac{1-\left(1-\pi_{ij}\right)^R}{\pi_{ij}} + R\left(1-\pi_{ij}\right)^R \quad (8)$$

Every attempt is charged to the transmitter through Eq. (1) and to the receiver through Eq. (3), whether or not it succeeds. This single modelling decision is what makes link-quality

awareness an energy question rather than a reliability question only. Figure 1 shows the resulting PRR against distance for three shadowing realisations; the usable range is roughly 90 m at the median and collapses under a 6 dB fade, so link quality varies substantially within a single deployment.

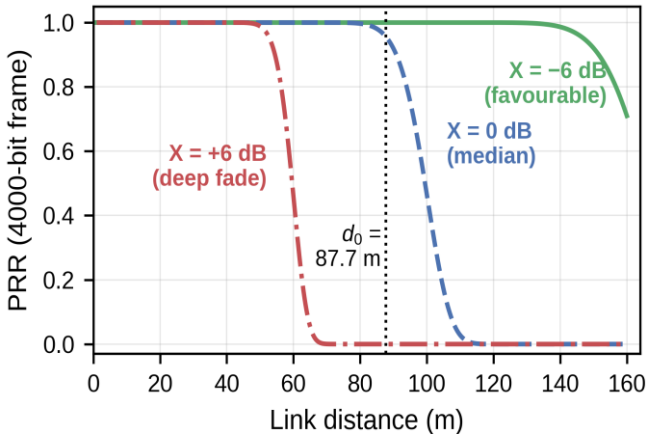


Figure 1. Packet reception ratio of a 4,000-bit frame against link distance

3.4 Correlation-aware aggregation

Readings from nearby nodes are redundant, so the compression achievable at a CH depends on the spatial compactness of its cluster [16]. With mean member distance $\bar{d}$ and correlation length θ, the aggregate emitted by a CH serving m members is modelled as:

$$\rho_c = \exp\left(-\bar{d}_c/\theta\right), \qquad b_c = k[1 + m_c(1 - \rho_c)] \tag{9}$$

A compact cluster therefore compresses well and a dispersed one barely compresses at all, which couples cluster geometry to forwarding cost and prevents the model from rewarding arbitrarily large clusters.

3.5 Problem statement

For each round, the protocol must choose a CH set, a member-to-CH assignment and a forwarding parent for every CH, so as to maximise the number of source readings delivered to the sink over the network lifetime per unit of energy consumed. The primary objective is therefore energy per delivered bit:

$$\eta = \frac{N\,E_0 - \sum_i E_i\,(\mathcal{R})}{k \sum_r |\mathcal{D}(r)|} \tag{10}$$

where, $D(r)$ is the set of readings delivered in round r and R is the set of rounds simulated. This normalised quantity is used in preference to residual energy, which rewards a protocol for not transmitting, and in preference to PDR alone, which rewards a protocol for transmitting wastefully.

4. THE UA-IT2F/AEO FRAMEWORK

4.1 Architecture and time scales

The framework separates two decisions that the surveyed schemes take together. Cluster formation is a relatively expensive combinatorial problem whose solution remains valid while the topology is stable, so it is solved every T_c rounds. Backbone routing is a shortest-path problem over a handful of CHs whose correct answer changes as soon as one relay's residual energy falls, so it is re-solved every round. Section 6.7 shows that this separation is one of the two mechanisms that actually carries the reported improvement. Figure 2 illustrates the resulting structure in the three evaluated scenarios.

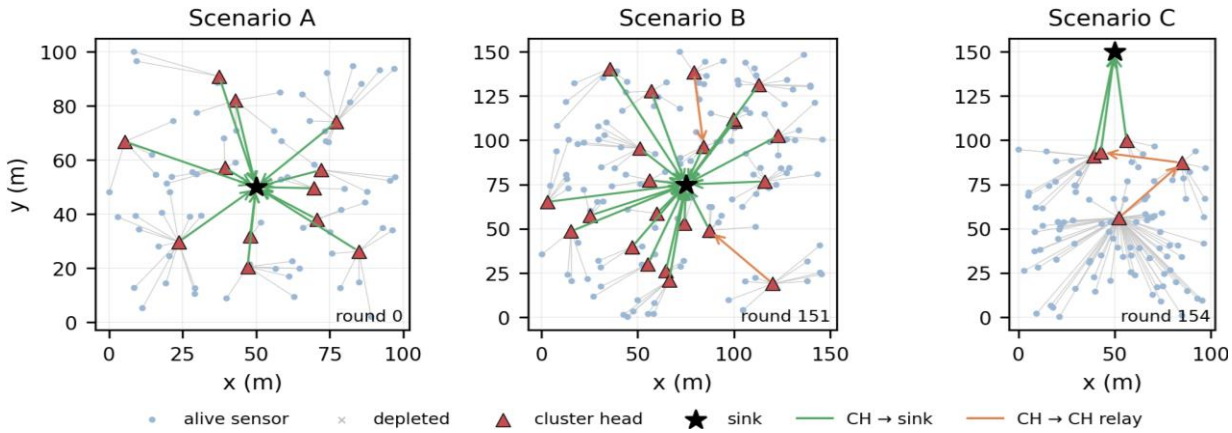


Figure 2. Cluster membership and backbone structure in the three scenarios

The panels of Figure 2 serve different illustrative purposes. Panel A shows the initial clustering at round 0, where the backbone is entirely single-hop because every head can reach the central sink directly. Panels B and C are taken in mid-life, at rounds 151 and 154, when depleted nodes have appeared and CH-to-CH relays are in use, which is the stage at which the multi-hop backbone is most informative. The panels are intended to show the structure of the solution - how many heads are formed, where they sit and how the backbone connects them - and not to support quantitative comparison between scenarios, which is given in Section 6.

The marked imbalance of cluster sizes in Scenario C has three causes that act together. First, with the sink outside the field the adaptive count of Eq. (23) yields few heads (3.7 on average; see Section 6.4), so each head must serve a large area. Second, CH-to-sink transmission is cheapest for heads near the sink-side edge, where the distance stays below d0 and the free-space term of Eq. (1) applies; the energy and backbone terms

of the fitness therefore draw several heads towards y = 90 m and leave the far half of the field to a single central head. Third, members are assigned to the head of minimum expected ARQ cost, and because link shadowing in Eq. (6) is formed from the two endpoint states, a head whose own shadowing state is favourable offers good links to all of its neighbours at once and attracts a disproportionate share of them. Nothing in the assignment limits cluster size; the fitness penalises the consequence only indirectly, through the poorer compression of a dispersed cluster in Eq. (9) and through the fairness term. Section 8 returns to this limitation.

4.2 Interval type-2 fuzzy decision module

Each candidate node i is scored by an aggregation suitability score computed from normalised residual energy, normalised distance to the sink and estimated link reliability:

$$ASS_i = \tilde{f}\left(\hat{E}_i, \hat{D}_i, \hat{R}_i\right) \in [0,1] \tag{11}$$

Interval type-2 inference has been applied to WSN clustering before, chiefly to size unequal clusters [41, 42]; here it scores aggregator suitability and, unlike those schemes, feeds its own uncertainty band back to the optimizer. The rule base contains the 27 rules obtained from all combinations of three linguistic terms per input, with triangular membership functions and five output levels, matching the structure used in the study [8] so that the comparison isolates the type-2 extension rather than the rule base. The inputs are not known exactly: reliability is an estimate from a finite and non-stationary sample, and the energy map is only as fresh as the last re-clustering. An interval type-2 system [17, 18] represents this by blurring each membership function into upper and lower bounds:

$$\begin{aligned} \overline{\mu}_A(x) &= \max_{|\delta|\le\Delta} \mu_A(x+\delta), \\ \underline{\mu}_A(x) &= \min_{|\delta|\le\Delta} \mu_A(x+\delta) \end{aligned} \tag{12}$$

The novelty here is that the blur half-width is not a design constant. For reliability it tracks the volatility of the estimator, measured by an exponentially weighted dispersion v of the observed PRR, together with sample scarcity through the observation count n:

$$\Delta_i^R = \mathrm{clip}\left(0.03 + 1.2\sqrt{v_i} + \frac{0.20}{\sqrt{1+n_i}},\ 0.03,\ 0.40\right) \tag{13}$$

Each term of Eq. (13) has a direct physical reading. The dispersion is updated after every observed frame exchange as $v_i \leftarrow (1 - \beta)\, v_i + \beta\, (\mathrm{PRR}_{obs} - \mathrm{rel}_i)^2$, where PRR_{obs} is the packet reception ratio observed in the current round, rel_i is the exponentially weighted reliability estimate and β, between 0 and 1, is the forgetting factor of the exponential weighting; the square root of v_i is therefore the recent standard deviation of the node's PRR, expressed in PRR units. The term $1.2\sqrt{(v_i)}$ sets the blur to a band of ± 1.2 standard deviations around the estimate, which would contain about 77% of PRR observations if their fluctuations were Gaussian; it represents genuine link volatility and does not shrink as observations accumulate. The term $0.20/\sqrt{(1 + n_i)}$ represents sample scarcity: it decays with the $1/\sqrt{(n)}$ law of the standard error of an estimated proportion, and its coefficient corresponds to half the standard error of a link with PRR near 0.8, for which $\sqrt{(0.8 \times 0.2)} = 0.4$. The floor of 0.03 is the residual imprecision that remains even for a stable, well-observed link, arising from the quantisation of the normalised inputs and from the staleness of the estimate between re-clustering events. The cap of 0.40 follows from the partition of the input universe. For three evenly spaced triangular terms on [0, 1], whose half-base is 0.5, the lower membership function of Eq. (12) peaks at 1 - 2Δ, so a half-width of 0.5 or more would make it vanish and leave y_l in Eq. (14) undefined; the cap keeps that peak at 0.2 or above. These values were fixed a priori from the above considerations and were not tuned on the evaluated scenarios.

A numerical example shows how the footprint reacts. Consider nodes with n = 24 reliability observations, for which the scarcity term is 0.20/5 = 0.040. A node on a stable link with $\sqrt{(v)} = 0.02$ receives $\Delta^R = 0.03 + 0.024 + 0.040 = 0.094$, whereas a node on a volatile link with $\sqrt{(v)} = 0.063$ ($v = 0.004$) receives $\Delta^R = 0.03 + 0.076 + 0.040 = 0.146$. A newly observed node (n = 0, v = 0) receives $\Delta^R = 0.230$ from scarcity alone, while the volatile node still retains $\Delta^R = 0.03 + 0.076 + 0.010 = 0.116$ after 399 observations, which is the non-collapse property discussed below. Suppose the stable and the volatile node have the same reliability estimate $\hat{R} = 0.80$. Under the 'high' reliability term, which rises linearly from 0.5 to 1, both have a type-1 membership of 0.60. With the dynamic footprint the stable node's membership becomes the interval [0.41, 0.79] and the volatile node's [0.31, 0.89]. The interval of the volatile node is 0.58 wide against 0.38 for the stable node, about 1.5 times wider, and the rule firing intervals inherit this difference. Because the footprint widens almost symmetrically about the type-1 membership on the linear part of a term, the upper and lower outputs of Eq. (14) move in opposite directions and their average changes little, whereas u in Eq. (15) grows directly with the width. For identical energy and distance inputs the two nodes therefore obtain almost the same suitability score, but the volatile node contributes a markedly larger uncertainty index. The uncertainty layer therefore acts mainly on the optimizer through Eq. (19) and only weakly on the score itself, which anticipates the null result of Section 6.7.

This matters because under correlated shadowing the uncertainty of a link estimate does not vanish as observations accumulate, so a count-based footprint would collapse the system to type-1 after a few hundred rounds. Firing strengths are computed separately on the upper and lower bounds and reduced in closed form by the Nie-Tan reducer [19], avoiding iterative Karnik-Mendel type reduction:

$$\begin{aligned} y_u &= \frac{\sum_q \overline{w}_q\, \vartheta_q}{\sum_q \overline{w}_q}, \\ y_l &= \frac{\sum_q \underline{w}_q\, \vartheta_q}{\sum_q \underline{w}_q}, \quad ASS_i = \frac{1}{2}(y_u + y_l) \end{aligned} \tag{14}$$

The normalised width of the firing interval is retained as a per-node uncertainty index and averaged over the network [20], and is fed to the optimizer:

$$u_i = \frac{\sum_q \overline{w}_q - \sum_q \underline{w}_q}{\sum_q \overline{w}_q}, \mathcal{U} = \frac{1}{N_a}\sum_i u_i \tag{15}$$

4.3 Uncertainty-aware adaptive Equilibrium Optimizer

Candidate solutions are real vectors in $[0,1]^{Na}$ whose largest components designate CHs. The EO update follows the original formulation [11], with an equilibrium pool of the four

best candidates plus their mean:

$$t = \left(1 - \frac{\tau}{T}\right)^{\frac{a_2 \tau}{T}}, \qquad \mathrm{F} = a_1 \,\mathrm{sgn}(\mathrm{r} - 0.5)\left(e^{-\lambda t} - 1\right) \tag{16}$$

$$\mathrm{G} = 0.5\, r_1\, 1[r_2 \geq GP]\left(\mathrm{C}_{eq} - \lambda \odot \mathrm{C}\right) \odot \mathrm{F} \tag{17}$$

$$\mathrm{C} \leftarrow \mathrm{C}_{eq} + \left(\mathrm{C} - \mathrm{C}_{eq}\right) \odot \mathrm{F} + \frac{\mathrm{G}}{\lambda V} \odot (1 - \mathrm{F}) \tag{18}$$

In the standard formulation the exploration gain a_1 and the generation probability GP are constants and the balance between exploration and exploitation is driven only by the iteration counter through t. Here they are re-tuned every iteration from three measured signals: normalised population diversity, a normalised stagnation counter, and the exogenous fuzzy uncertainty index of Eq. (15).

$$\psi = 0.5\left(1 - \hat{\Sigma}\right) + 0.3\,\hat{\zeta} + 0.2\,\mathcal{U} \tag{19}$$

$$a_1 = a_1^0(0.6 + 0.9\psi), \qquad GP = \mathrm{clip}(0.75 - 0.5\psi,\ 0.2,\ 0.8) \tag{20}$$

The intent is that the search explores more when its population has collapsed, when it has stopped improving, or when the evidence on which the fuzzy scores rest is itself weak. Section 6.7 reports that this mechanism does not yield a measurable network-level benefit.

The three signals do not contribute equally. By construction of Eq. (19), population diversity can move ψ by at most 0.5, stagnation by at most 0.3 and the fuzzy uncertainty index by at most 0.2; through Eq. (20) the full range of ψ maps a_1 to between $0.6a_1{}^0$ and $1.5a_1{}^0$ and GP to between 0.75 and 0.25. The uncertainty index is computed once per re-clustering event (Algorithm 1, line 4) and is constant throughout the subsequent optimizer run, so within a run it acts only as a fixed offset to ψ; diversity and stagnation are the only signals that vary from iteration to iteration. Section 6.6 discusses, alongside the optimizer convergence curves, why this adjustment has little measurable effect under the tested conditions.

4.4 Fitness function

Each candidate is evaluated by simulating one round analytically. Predicted energy uses Eq. (1) weighted by the expected ARQ transmission count of Eq. (8), so unreliable assignments are penalised through their true cost. Predicted delivery multiplies the member hop success probability by the end-to-end success of the CH's path. Load balance is measured by Jain's fairness index [43] over predicted post-round residual energies:

$$\mathcal{J} = \frac{(\sum_i E_i)^2}{N_a \sum_i E_i^2} \tag{21}$$

A rotation term, measuring how long each selected node has been idle since it last served as a CH, counteracts the tendency of an informed election to re-select the same well-placed nodes until they fail. The composite objective, minimised, is:

$$\Phi = 0.34\,\hat{\mathcal{E}} + 0.28\left(1 - \hat{P}\right) + 0.20(1 - \mathcal{J}) + 0.06\,\hat{D} + 0.04\left(1 - \overline{ASS}\right) + 0.10(1 - \bar{\mathrm{Q}}) \tag{22}$$

The weights were fixed once, before the experiments, from a priority ordering of the objectives rather than by numerical tuning, and no scenario-specific tuning is performed anywhere in this study. All six terms are normalised to [0, 1], so the weights express relative importance directly. The two terms that make up the primary figure of merit of Eq. (10), predicted energy (0.34) and predicted delivery (0.28), together receive 0.62; energy is weighted slightly higher because it is the numerator of η and is consumed irreversibly. The two lifetime-protection terms, fairness (0.20) and rotation (0.10), receive 0.30; fairness is weighted above rotation because it acts on the predicted energy of every node, whereas rotation acts only on the selected heads. The distance term (0.06) and the mean suitability score (0.04) act as tie-breakers between assignments that are otherwise equivalent in cost. One consequence of this ordering is that the fuzzy score enters the objective only weakly and influences the search mainly through the seeding of the initial population (Algorithm 1, line 5), which is relevant to the interpretation of the ablation in Section 6.7. Section 6.8 reports a sensitivity check on the two weights most likely to alter CH selection.

Algorithm 1. UA-IT2F/AEO, one communication round r

Input: node positions, residual energies E, link statistics (rel, v, n), round r
Output: readings delivered to the sink; updated energies
1: if r mod T_c = 0 or any CH is dead then
2: N_a ← |alive|; m ← k_{opt} by Eq. (23)
3: compute normalised E, D, R; FOU half-widths by Eq. (13)
4: (ASS, u) ← IT2 inference, Eqs. (12)–(15)
5: C ← init population seeded from ASS
6: for τ = 1 to T do
7: ψ ← diversity, stagnation, U; a_1, GP by Eqs. (19)–(20)
8: update C by Eqs. (16)–(18); evaluate Φ by Eq. (22)
9: CH ← top-m components of the best solution
10: assign each member to argmin expected ARQ cost
11: end if
12: backbone ← Dijkstra over CH with edge cost Eqs. (24)–(25) // every round
13: members transmit to their CH under truncated ARQ; charge Eqs. (1) and (3)
14: each CH aggregates; output size by Eq. (9)
15: forward aggregates along the backbone, deepest CH first
16: update rel, v, n from observed PRR; mark depleted nodes dead

4.5 Adaptive cluster count

The classical optimum number of clusters assumes that every CH transmits directly to the sink, which over-penalises distant CHs when a backbone exists. We therefore cap the sink-ward distance entering the expression at the crossover distance d_0, beyond which relaying is always cheaper than direct transmission, and clip the result to a practical band recomputed from the surviving node count:

$$k_{opt} = \mathrm{clip}\left(\sqrt{\frac{N_a}{2\pi}}\,\sqrt{\frac{\varepsilon_{fs}}{\varepsilon_{mp}}}\,\frac{M}{d_{eff}^2},\ 0.05N_a,\ 0.15N_a\right) \tag{23}$$

4.6 Energy- and reliability-aware backbone

Given the CH set, a directed graph is built in which an edge is admissible only if it moves strictly closer to the sink, which prevents loops and detours. Edge cost combines expected ARQ energy, a reliability penalty and a residual-energy penalty computed relative to the mean CH energy, so that a relay is avoided before it is exhausted rather than after:

$$w(c,c') = [E_{tx}(b,d_{cc'})\mathbb{E}[T_{cc'}] + E_{rx}(b)] \\ \left(1 + 2(1 - P^{s}_{cc'})\right) + \Omega_{c'} \quad (24)$$

$$\Omega_{c'} = 0.60\,\overline{w}_{sink}\left[\left(E_{c'}/\overline{E}\right)^{-2} - 1\right] \quad (25)$$

Parents are then obtained by a Dijkstra pass rooted at the sink. Because this pass is cheap it is repeated every round, which is what allows the sink-adjacent head to rotate within a clustering interval.

4.7 Algorithm and complexity

Per re-clustering event the optimizer costs O(P × I × N_a × m) for population P, I iterations, N_a alive nodes and m CHs; the fuzzy module is O(N_a) since all 27 rules are evaluated in vectorised form. The per-round cost is dominated by member assignment, O(N_a × m), and the backbone pass, O(m^2 log m). With the settings of Section 5.1 the optimizer runs once per 10 rounds and the round cost is linear in the number of surviving nodes.

5. EXPERIMENTAL METHODOLOGY

5.1 Scenarios and parameters

Three scenarios are used. Scenario A reproduces the configuration of the closest antecedent [8] - a 100 m × 100 m field with 80 nodes and a central sink - so that results are comparable with published practice. Scenario B enlarges the field and the population to 150 m × 150 m and 150 nodes, placing a substantial fraction of nodes beyond the crossover distance d_0. Scenario C keeps 100 m × 100 m and 100 nodes but moves the sink to (50, 150), outside the field, which is the standard stress test for single-hop clustering. Parameters are listed in Table 2 and are identical for every protocol.

5.2 Baselines

Four baselines are reimplemented inside the same simulator, sharing the identical energy, channel, ARQ and aggregation accounting, so that differences arise only from clustering and routing decisions. Because the published algorithms were evaluated under different channel and energy models, most of them without frame loss, the reimplemented versions are reproductions rather than the original implementations, and their behaviour may differ from that reported in the original studies. Throughout this paper the names LEACH, Fuzzy-LEACH, EEO and FCEO denote these reproductions, and their results should not be read as a re-run of the published experiments. Table 3 separates, for each baseline, what is retained from the published algorithm from what was adapted to the common model, and lists the principal implementation settings. LEACH [1] uses the standard probabilistic threshold with rotation. Fuzzy-LEACH follows Gupta et al. [6], electing heads by a Mamdani system over energy, concentration and centrality with rotation pressure. EEO is the enhanced Equilibrium Optimizer baseline used in the study [8], in which the enhanced EO update of the study [26] selects heads under an energy-delay-reliability fitness with single-hop forwarding. FCEO is our reproduction of the study [8]: a type-1 Mamdani suitability score biasing an EO search, with a three-level node-CH-gateway-sink hierarchy.

The gateway election and forwarding rules of FCEO are described in the original study [8] at the level of the hierarchy, so the following explicit rules were adopted in the reproduction. At every re-clustering event the CHs are ranked by their type-1 suitability score and the highest-scoring quarter, rounded up and never fewer than one, are designated gateways. Each non-gateway CH forwards its aggregate in a single hop to its nearest gateway, and each gateway transmits its own aggregate together with the received aggregates directly to the sink. Gateways are not re-elected between re-clustering events, so a gateway whose energy declines continues to relay until the next event. This fixed relay layer is the feature examined in Sections 6.5 and 7.3.

5.3 Metrics

Lifetime is reported as first node death (FND), half node death (HND) and last node death (LND) rather than a single figure, because these can and do disagree. Efficiency is reported as energy per delivered bit, Eq. (10). Reliability is reported as the fraction of generated readings that reach the sink. Jain's index over residual energies measures load balance, and transmissions per delivered packet exposes retransmission overhead.

Table 2. Simulation parameters

Parameter	Value	Parameter	Value
Field (A/B/C)	100 × 100/150 × 150/100 × 100 m	Packet size k	4,000 bits
Nodes N (A/B/C)	80/150/100	E_{elec}	50 nJ/bit
Sink (A/B/C)	(50, 50)/(75, 75)/(50, 150)	ε_{fs}	10 pJ/bit/m^2
Initial energy E_0	0.5 J	ε_{mp}	0.0013 pJ/bit/m^4
Crossover distance d_0	87.7 m	E_{DA}	5 nJ/bit
Transmit power P_t	0 dBm	Noise floor P_n	-104 dBm
Path loss PL_0/n	42 dB/2.7	Shadowing sigma	6 dB
Shadowing AR(1) rho	0.7	Max ARQ attempts R	3
Correlation length θ	40 m	Re-clustering period T_c	10 rounds
EO population	20	EO iterations	15
Baseline CH ratio	5%	Adaptive CH band	5–15% of alive nodes
Seeds (main/ablation/sweep)	20/15/10	Max rounds	6,000

Table 3. Published baseline algorithms and the reproductions evaluated in this study

Baseline	Source	Retained from the Published Algorithm	Adapted in This Reproduction	Principal Settings
LEACH	[1]	Probabilistic threshold election with epoch-based rotation; members join a head; single-hop CH-to-sink transmission	Common channel, truncated ARQ and correlation-aware aggregation	Desired CH ratio 5%; election every round
Fuzzy-LEACH	[6]	Mamdani election from residual energy, node concentration and centrality; single-hop CH-to-sink transmission	Rotation pressure added to avoid repeated election of the same nodes; common model	CH ratio 5%; election every round
EEO	[8, 26]	EO-based head selection with the enhanced update of the study [26]; energy-delay-reliability fitness of the EEO baseline in the study [8]; single-hop forwarding	Common model; EO budget aligned with the proposal	Population 20, 15 iterations; CH ratio 5%; T_c = 10 rounds
FCEO	[8]	27-rule type-1 Mamdani suitability score; EO search biased by the score; node-CH-gateway-sink hierarchy	Gateway election and forwarding rules made explicit (Section 5.2); common model	Population 20, 15 iterations; CH ratio 5%; T_c = 10 rounds; gateways = top quarter of heads
UA-IT2F/AEO	This work	-	-	Population 20, 15 iterations; CH band 5-15% of alive nodes; T_c = 10 rounds; backbone every round

Note: All four baselines share the channel, ARQ, energy and aggregation model of Section 3. FCEO: Fuzzy-Controlled Equilibrium Optimizer; Low-Energy LEACH: Low-Energy Adaptive Clustering Hierarchy.

5.4 Statistical protocol

Each protocol is run on 20 independently generated deployments per scenario, using the same 20 random seeds for every protocol so that comparisons are paired. The ablation uses 15 seeds and the density sweep 10. Following standard practice for comparing algorithms over multiple problem instances [44], we use the Friedman test across all five protocols, then paired one-sided Wilcoxon signed-rank tests [45] of the proposal against each baseline, with Holm correction [46] within each metric, and report Cliff's delta [47] as a non-parametric effect size.

6. RESULTS

6.1 Survivability

Figure 3 shows the number of alive nodes against round, averaged over 20 deployments, and Figure 4 the distribution of HND. UA-IT2F/AEO sustains the network markedly longer in the central-sink scenarios: HND rises from 836 rounds for the best baseline to 1,018 in Scenario A (+21.8%) and from 773 to 926 in Scenario B (+19.8%). In the offset-sink Scenario C the margin narrows to +9.0% over EEO. FND improves more sharply still, from 310 to 529 rounds in Scenario A, because the fairness and rotation terms delay the first failure rather than merely prolonging the tail.

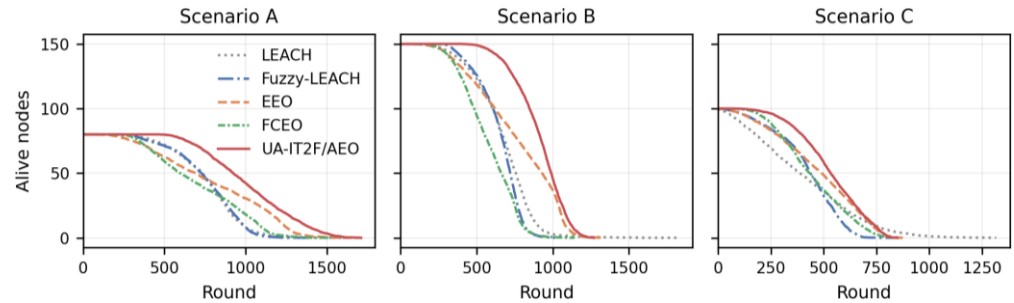


Figure 3. Alive nodes against simulation round (mean of 20 deployments)

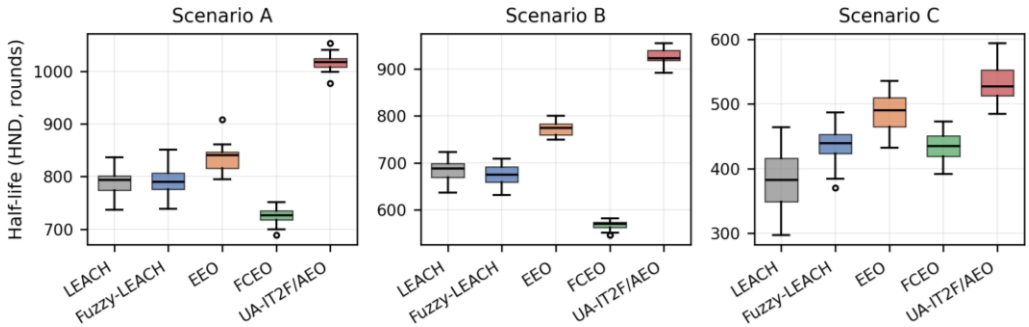


Figure 4. Distribution of half node death (HND) over 20 deployments

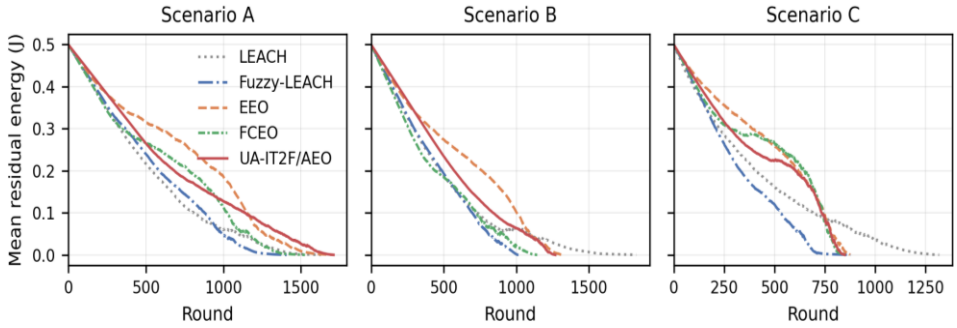


Figure 5. Mean residual energy per surviving node against round

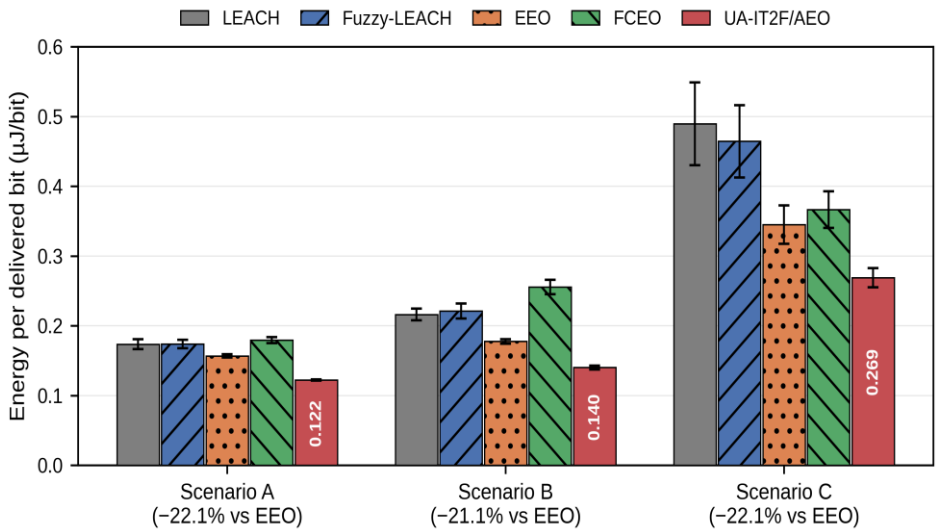


Figure 6. Energy per delivered bit of all protocols (mean ± standard deviation)

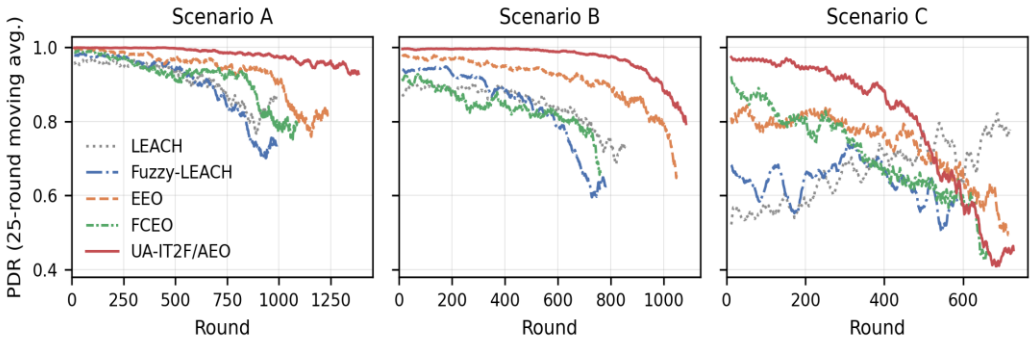


Figure 7. Packet delivery ratio (PDR) against round (25-round moving average)

Table 4. Performance of all protocols in the three scenarios

Scenario A - 100 m × 100 m, N = 80, central sink

Protocol	FND	HND	LND	PDR	Energy/bit (µJ)	Avg. Alive	Tx/Delivered pkt	Jain Index	CHs
LEACH	231 ± 80	788 ± 25	1,341	0.9309 ± 0.0089	0.1737 ± 0.0070	46.5	1.87	0.835	2.3
Fuzzy-LEACH	310 ± 23	791 ± 28	1,186	0.9308 ± 0.0079	0.1739 ± 0.0059	52.2	1.74	0.867	2.7
EEO	166 ± 42	836 ± 26	1,474	0.9588 ± 0.0018	0.1568 ± 0.0023	45.2	1.49	0.896	2.4
FCEO	266 ± 27	726 ± 16	1,322	0.9411 ± 0.0062	0.1794 ± 0.0044	44.9	1.60	0.876	2.4
UA-IT2F/AEO	529 ± 37	1,018 ± 17	1,609	0.9888 ± 0.0009	0.1222 ± 0.0009	51.4	1.08	0.839	7.5

Scenario B - 150 m × 150 m, N = 150, central sink

Protocol	FND	HND	LND	PDR	Energy/bit (µJ)	Avg. Alive	Tx/Delivered pkt	Jain Index	CHs
LEACH	171 ± 72	685 ± 22	1,348	0.8665 ± 0.0110	0.2162 ± 0.0085	75.6	1.99	0.830	3.8
Fuzzy-LEACH	296 ± 25	674 ± 23	948	0.8752 ± 0.0132	0.2212 ± 0.0108	102.4	2.29	0.858	5.0
EEO	162 ± 32	773 ± 15	1,221	0.9351 ± 0.0051	0.1776 ± 0.0033	92.5	1.67	0.873	4.6
FCEO	173 ± 59	568 ± 11	984	0.8564 ± 0.0144	0.2556 ± 0.0103	87.5	2.38	0.839	4.4
UA-IT2F/AEO	486 ± 38	926 ± 17	1,218	0.9826 ± 0.0017	0.1402 ± 0.0028	111.6	1.20	0.843	13.3

Scenario C - 100 m × 100 m, N = 100, sink at (50, 150)

Protocol	FND	HND	LND	PDR	Energy/bit (µJ)	Avg. Alive	Tx/Delivered pkt	Jain Index	CHs
LEACH	8 ± 5	386 ± 44	1,115	0.6292 ± 0.0343	0.4896 ± 0.0595	36.8	5.58	0.812	2.2
Fuzzy-LEACH	46 ± 33	436 ± 31	697	0.6450 ± 0.0310	0.4645 ± 0.0519	60.3	5.15	0.798	2.9
EEO	37 ± 17	487 ± 29	800	0.7693 ± 0.0208	0.3450 ± 0.0276	58.9	4.25	0.910	2.8
FCEO	113 ± 41	434 ± 23	773	0.7649 ± 0.0216	0.3667 ± 0.0263	57.7	6.71	0.883	2.8
UA-IT2F/AEO	143 ± 32	531 ± 27	790	0.8742 ± 0.0127	0.2689 ± 0.0138	67.2	4.20	0.832	3.7

Notes: Values are mean ± standard deviation over 20 deployments; FND, HND and LND are given in rounds; the baselines are the reproductions described in Section 5.2. Note: FND: first node death, HND: half node death, LND: last node death, CHs: cluster heads, FCEO: Fuzzy-Controlled Equilibrium Optimizer; LEACH: Low-Energy Adaptive Clustering Hierarchy.

LND behaves differently and deserves comment. In Scenario C, LEACH records the longest LND of any protocol, 1,115 rounds against 791 for the proposal, yet its first node dies at round 8 and it delivers only 62.9% of readings. What LND is measuring there is not endurance but extreme imbalance: a handful of nodes near the sink survive long after the network has ceased to cover the field. A protocol that balances energy necessarily compresses the interval between first and last death, which depresses LND. Reporting LND alone would invert the ranking, and this is a concrete reason to report the triple.

6.2 Energy efficiency

Figure 5 shows mean residual energy against round and Figure 6 energy per delivered bit. The two tell deliberately different stories. Under residual energy, EEO retains more energy than the proposal through much of the lifetime in all three scenarios; taken alone this would suggest EEO is the more efficient protocol. Energy per delivered bit shows the opposite: 0.1222 µJ/bit against 0.1568 in Scenario A (-22.1%), 0.1402 against 0.1776 in Scenario B (-21.1%) and 0.2689 against 0.3450 in Scenario C (-22.1%). EEO conserves energy partly by delivering less. Retransmission counts confirm the mechanism: the proposal needs 1.08 transmissions per delivered packet in Scenario A against 1.49 for EEO and 1.87 for LEACH, and 4.20 against 6.71 for FCEO in Scenario C.

All relative figures in this paper are computed directly from the means in Table 4. The reductions quoted above are relative to the strongest baseline on this metric, which is EEO in all three scenarios, and give the 21.1-22.1% range used in the abstract and conclusions. Relative to the weakest baseline the reductions are larger: 31.9% against FCEO in Scenario A, 45.1% against FCEO in Scenario B and 45.1% against LEACH in Scenario C.

6.3 Delivery reliability

Figure 7 shows PDR smoothed over 25 rounds and truncated once fewer than 10% of nodes survive, since PDR is meaningless in a nearly dead network. The proposal holds the highest delivery ratio throughout the useful lifetime in every scenario, averaging 0.9888, 0.9826 and 0.8742 against best-baseline values of 0.9588, 0.9351 and 0.7693. The gap is widest in Scenario C, where single-hop protocols must cross distances at which the PRR of Figure 1 has already collapsed and therefore exhaust their ARQ budget.

6.4 Aggregate results and significance

Table 4 collects the full set of scalar metrics. The Friedman test rejects the hypothesis of equal performance across the five protocols for PDR, energy per bit and HND in every scenario ($p < 6 \times 10^{-15}$). Table 5 reports the paired comparisons of the proposal against each baseline.

Every comparison is significant after correction, with $p \leq 1.8 \times 10^{-4}$ throughout, and effect sizes are uniformly large: Cliff's delta reaches its maximum of 1.00 for PDR and energy per bit in all three scenarios, meaning that every one of the 20 paired deployments favours the proposal. The single value below 1.00 is HND against EEO in Scenario C (delta = 0.72), which remains a large effect.

6.5 Scalability

Figure 8 sweeps the node count from 50 to 200 in a fixed 150 m × 150 m field. The proposal improves monotonically with density, from PDR 0.957 at N = 50 to 0.985 at N = 200,

because a denser field offers shorter member links and more relay candidates. FCEO moves in the opposite direction, from 0.893 to 0.851, and its energy per bit is essentially flat at about 0.25 µJ/bit: its fixed quarter-of-heads gateway layer becomes a bottleneck as traffic grows, which is precisely the scalability limitation that a fixed hierarchy invites.

6.6 Optimizer convergence

Figure 9 shows the improvement of the best fitness over the initial population, normalised per algorithm because the three optimizers minimise different objectives and their raw values are not comparable. The magnitudes are small. In Scenario B the search improves its own starting point by 1.9% (EEO), 3.1% (FCEO) and 1.7% (the proposal); in Scenario C by 17.2%, 1.7% and 2.8%. The fuzzy-seeded methods begin near their final solution, so the metaheuristic contributes little refinement. This is the first indication that the optimizer may not be the source of the observed gains, and it motivates Section 6.7.

Table 5. Paired Wilcoxon signed-rank tests of UA-IT2F/AEO against each baseline

Metric	Scenario	vs LEACH	vs Fuzzy-LEACH	vs EEO	vs FCEO
PDR	A	$p = 3.8 \times 10^{-6}$, d = +1.00	$p = 3.8 \times 10^{-6}$, d = +1.00	$p = 3.8 \times 10^{-6}$, d = +1.00	$p = 3.8 \times 10^{-6}$, d = +1.00
	B	$p = 3.8 \times 10^{-6}$, d = +1.00	$p = 3.8 \times 10^{-6}$, d = +1.00	$p = 3.8 \times 10^{-6}$, d = +1.00	$p = 3.8 \times 10^{-6}$, d = +1.00
	C	$p = 3.8 \times 10^{-6}$, d = +1.00	$p = 3.8 \times 10^{-6}$, d = +1.00	$p = 3.8 \times 10^{-6}$, d = +1.00	$p = 3.8 \times 10^{-6}$, d = +1.00
Energy per bit	A	$p = 3.8 \times 10^{-6}$, d = -1.00	$p = 3.8 \times 10^{-6}$, d = -1.00	$p = 3.8 \times 10^{-6}$, d = -1.00	$p = 3.8 \times 10^{-6}$, d = -1.00
	B	$p = 3.8 \times 10^{-6}$, d = -1.00	$p = 3.8 \times 10^{-6}$, d = -1.00	$p = 3.8 \times 10^{-6}$, d = -1.00	$p = 3.8 \times 10^{-6}$, d = -1.00
	C	$p = 3.8 \times 10^{-6}$, d = -1.00	$p = 3.8 \times 10^{-6}$, d = -1.00	$p = 3.8 \times 10^{-6}$, d = -1.00	$p = 3.8 \times 10^{-6}$, d = -1.00
HND	A	$p = 1.8 \times 10^{-4}$, d = +1.00	$p = 1.8 \times 10^{-4}$, d = +1.00	$p = 1.8 \times 10^{-4}$, d = +1.00	$p = 1.8 \times 10^{-4}$, d = +1.00
	B	$p = 1.8 \times 10^{-4}$, d = +1.00	$p = 1.8 \times 10^{-4}$, d = +1.00	$p = 1.8 \times 10^{-4}$, d = +1.00	$p = 1.8 \times 10^{-4}$, d = +1.00
	C	$p = 1.8 \times 10^{-4}$, d = +1.00	$p = 1.8 \times 10^{-4}$, d = +0.99	$p = 1.8 \times 10^{-4}$, d = +0.72	$p = 1.8 \times 10^{-4}$, d = +1.00

Notes: One-sided tests over n = 20 deployments, Holm-corrected within each metric; d is the Cliff's delta effect size. PDR: packet delivery ratio, HND: half node death; LEACH: Low-Energy Adaptive Clustering Hierarchy.

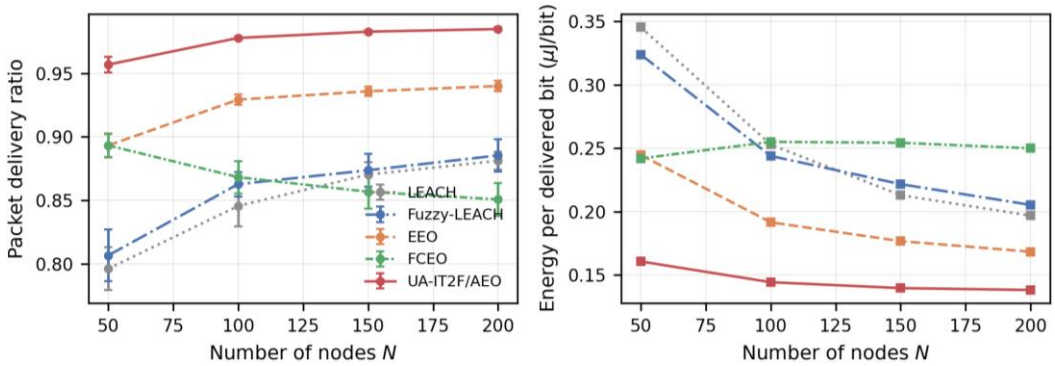


Figure 8. Delivery ratio and energy per delivered bit against node density

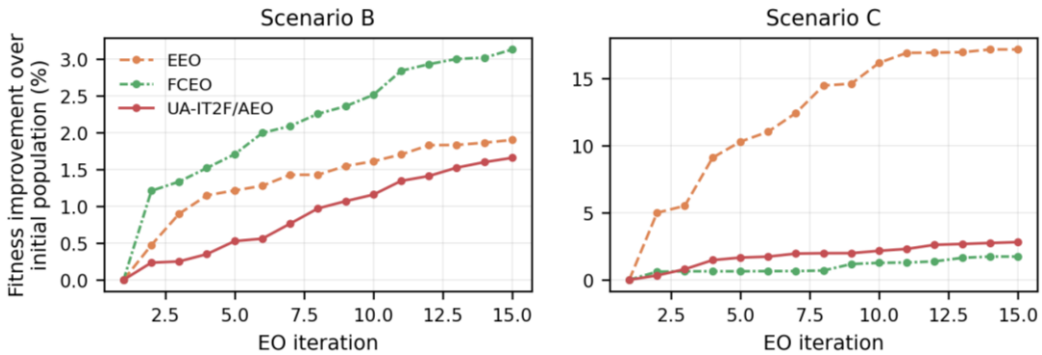


Figure 9. Fitness improvement over the initial population within one optimizer run

Figure 9 also explains why the uncertainty-aware controller of Section 4.3 has little measurable effect under the tested conditions. The controller acts only on the iterative refinement phase of the search, adjusting a_1 and GP as the run proceeds, and in the fuzzy-seeded methods that phase improves the best fitness by only 1.7–3.1% over the initial population. Whatever the controller does, its effect on the network is bounded by this small margin. Three features of the tested conditions shrink it further. First, each run has only 15 iterations, so the stagnation counter has little time to accumulate and the diversity signal little time to act. Second, the uncertainty index is fixed during a run (Section 4.3) and, being a network average, changes little between consecutive re-clustering events, so it shifts a_1 and GP by an almost constant amount that the iteration-driven schedule of Eq. (16) largely masks. Third, a candidate is decoded by taking its top-m components, so many different real vectors map to the same CH set, and modest changes in exploration pressure often leave the selected heads unchanged.

This interpretation is consistent with the greedy-ranking variant of Section 6.7, which costs 14.9% and 14.7% in energy

per bit. That penalty reflects the evaluation of a diverse, fuzzy-seeded population under the full fitness, which rejects the pathological selections that a greedy ranking makes; it does not depend on the iterative refinement on which the controller acts. The controller would be expected to matter only in larger or more rugged search spaces, for example with many more candidate heads or a longer optimisation budget, which this study does not test.

6.7 Component-level attribution

Eight variants were compared against the full model on the same 15 deployments: each of the five proposed mechanisms removed in turn, the optimizer replaced by a greedy ranking of the fuzzy scores, and CH election replaced by uniform random selection while retaining the rest of the architecture. Figure 10 and Table 6 report the outcome.

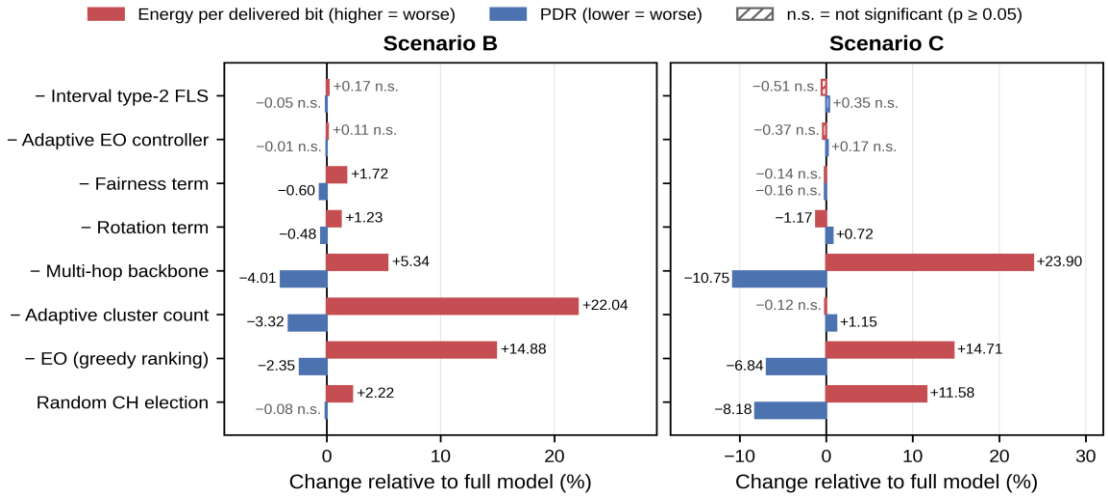


Figure 10. Change in energy per delivered bit and packet delivery ratio (PDR) when each component is removed

Table 6. Component-level ablation results

Variant Removed	Scen.	FND	PDR	dPDR (%)	p(PDR)	Energy/bit (µJ)	dE (%)	p(E)	Verdict
Full model	B	486	0.9828	-	-	0.1401	-	-	-
Interval type-2 FLS	B	464	0.9823	-0.05	0.12	0.1404	+0.17	0.064	no effect
Adaptive EO controller	B	465	0.9827	-0.01	0.60	0.1403	+0.11	0.15	no effect
Fairness term	B	337	0.9768	-0.60	6.1×10^{-5}	0.1426	+1.72	6.1×10^{-5}	significant
Rotation term	B	347	0.9780	-0.48	6.1×10^{-5}	0.1419	+1.23	6.1×10^{-5}	significant
Multi-hop backbone	B	429	0.9434	-4.01	6.1×10^{-5}	0.1476	+5.34	6.1×10^{-5}	significant
Adaptive cluster count	B	303	0.9501	-3.32	6.1×10^{-5}	0.1710	+22.04	6.1×10^{-5}	significant
EO (greedy ranking)	B	518	0.9596	-2.35	6.1×10^{-5}	0.1610	+14.88	6.1×10^{-5}	significant
Informed election (random)	B	485	0.9820	-0.08	0.14	0.1433	+2.22	6.1×10^{-5}	energy only
Full model	C	139	0.8748	-	-	0.2676	-	-	-
Interval type-2 FLS	C	134	0.8778	+0.35	0.33	0.2662	-0.51	0.39	no effect
Adaptive EO controller	C	142	0.8762	+0.17	0.93	0.2666	-0.37	0.72	no effect
Fairness term	C	121	0.8734	-0.16	0.64	0.2672	-0.14	0.85	no effect
Rotation term	C	135	0.8810	+0.72	0.035	0.2645	-1.17	0.048	slightly harmful
Multi-hop backbone	C	106	0.7807	-10.75	6.1×10^{-5}	0.3316	+23.90	6.1×10^{-5}	significant
Adaptive cluster count	C	139	0.8848	+1.15	0.015	0.2673	-0.12	1.00	slightly harmful
EO (greedy ranking)	C	250	0.8149	-6.84	6.1×10^{-5}	0.3070	+14.71	6.1×10^{-5}	significant
Informed election (random)	C	92	0.8032	-8.18	6.1×10^{-5}	0.2986	+11.58	6.1×10^{-5}	significant

Notes: 15 deployments; changes are relative to the full model; p-values are from paired two-sided Wilcoxon signed-rank tests against the full model. PDR: packet delivery ratio, EO: Equilibrium Optimizer, FLS: fuzzy logic system, FND: first node death.

The result is clear and only partly favourable. Two mechanisms carry the improvement. Removing the adaptive cluster count raises energy per bit by 22.0% in Scenario B ($p = 6.1 \times 10^{-5}$); removing the multi-hop backbone raises it by 5.3% in Scenario B and 23.9% in Scenario C and costs 4.0 and 10.8 percentage points of PDR respectively (all $p = 6.1 \times 10^{-5}$).

The fairness and rotation terms matter chiefly for early deaths: without rotation, FND in Scenario B falls from 486 to 347 rounds, and without the fairness term to 337.

The two components named in the framework's acronym do not survive testing. Replacing the interval type-2 system with its type-1 counterpart changes PDR by -0.05% in Scenario B and +0.35% in Scenario C, neither significant ($p = 0.12$ and 0.33). Disabling the uncertainty-aware optimizer controller changes PDR by -0.01% and +0.17%, also not significant ($p = 0.60$ and 0.93). We report these as null results.

Sections 4.4 and 6.6 give complementary reasons for these null results. The fuzzy score enters the fitness with a weight of only 0.04, so the type-2 layer can affect CH selection mainly through the seeding of the initial population, where, as the example of Section 4.2 shows, the type-1 and type-2 scores differ little. The adaptive controller acts on a refinement phase that improves fitness by only a few per cent. Neither layer therefore has much leverage over the decisions that the cluster count and the backbone have already largely determined.

The most instructive variant is random CH election. In the symmetric Scenario B it is statistically indistinguishable from informed election on PDR (0.9820 against 0.9828, $p = 0.14$), although it does cost 2.2% in energy per bit. In the asymmetric Scenario C the picture reverses sharply: random election loses 8.2 percentage points of PDR and 11.6% in energy per bit (both $p = 6.1 \times 10^{-5}$). Informed election, in other words, earns its cost only when the deployment geometry makes head placement consequential. Removing the optimizer entirely in favour of a greedy fuzzy ranking is worse than either, costing 14.9% and 14.7% in energy per bit, which indicates that what the search provides is mainly the avoidance of pathological greedy selections rather than fine optimisation.

6.8 Sensitivity to the fitness weights

To check whether the findings depend on the particular weights of Eq. (22), the energy weight and the fairness weight were each varied by ± 0.10 about their default values on 10 deployments of Scenario B, with the remaining weights rescaled proportionally so that all six still sum to one. These two weights were chosen because energy is the largest term and drives the cost-based selection of heads most directly, whereas fairness is the term that the ablation identifies as controlling early node death. Table 7 reports the outcome.

Table 7. Sensitivity of UA-IT2F/AEO to the energy and fairness weights (Scenario B)

Setting	w_E	w_J	FND	PDR	Energy/bit (µJ)	dE (%)
Default	0.34	0.20	[ ]	[ ]	[ ]	-
w_E - 0.10	0.24	0.224	[ ]	[ ]	[ ]	[ ]
w_E + 0.10	0.44	0.165	[ ]	[ ]	[ ]	[ ]
w_J - 0.10	0.373	0.10	[ ]	[ ]	[ ]	[ ]
w_J + 0.10	0.290	0.30	[ ]	[ ]	[ ]	[ ]
EEO (reference)	-	-	[ ]	[ ]	[ ]	[ ]

Notes: 10 deployments; the remaining weights are rescaled proportionally so that all weights sum to one. FND: first node death, PDR: packet delivery ratio.

Table 8. Analytical estimate of control-message overhead for UA-IT2F/AEO

Scenario	Frames per Routing Update	Frames per Re-Clustering Event	Control Energy per Round (mJ)	Share of Data Energy (%)	Energy/Bit incl. Control (µJ)	Advantage over EEO (%): Reported/with Control
A	1–15	52–66	0.33–0.57	1.3–2.3	0.1238–0.1250	22.1/20.3–21.0
B	1–27	113–138	0.81–1.41	1.3–2.3	0.1421–0.1434	21.1/19.3–20.0
C	1–15	72–82	0.37–1.12	0.6–1.8	0.2705–0.2737	22.1/20.7–21.6

Notes: Each range gives the lower and the upper estimate; the assumptions are stated in Section 6.9.

6.9 Estimated control-message overhead

The results above, like those of the baselines, charge no energy for disseminating clustering and routing decisions. Because the proposal re-solves the backbone every round, this omission could favour it, so the overhead is estimated here analytically under the radio, channel and ARQ model of Section 3. A centralised implementation in the manner of LEACH-C [2] is assumed, in which the sink, which is not energy constrained, runs the optimizer and the Dijkstra pass, and every control frame carries a 200-bit header and identifier field, of the order of a short IEEE 802.15.4 frame [48].

A routing update requires the residual energy of each CH at the sink and returns one parent identifier to each CH. In the lower estimate the 16-bit energy field is piggybacked on the CH's data aggregate, and the sink broadcasts the m parent identifiers in a single frame received by every CH, so only one additional frame is transmitted per round. In the upper estimate each CH sends a separate report along its backbone path and the parent assignment is relayed back hop by hop, which costs 2m frames per backbone hop. A re-clustering event additionally requires a status frame from every member to its head (energy, reliability, dispersion and observation count, 40 bits per node), one combined report per cluster forwarded along the backbone, and dissemination of the new CH set, by a single sink broadcast in the lower estimate and by relay and rebroadcast through every head in the upper estimate. Re-clustering is assumed to occur every 10 rounds in the lower estimate and, to allow for off-schedule triggers, every 5 rounds in the upper estimate. Every control frame is charged through Eqs. (1) and (3) and multiplied by its expected number of ARQ attempts from Eq. (8) at the corresponding hop distance, averaged over the shadowing distribution. Member and backbone hop distances are taken from the mean geometry of each scenario with the average numbers of alive nodes and heads in Table 4, and the data energy per round is obtained as energy per delivered bit multiplied by the bits delivered per round.

Table 8 summarises the estimate. A routing update needs between 1 and 27 additional frames per round and a re-clustering event between 52 and 138, depending on the scenario and the assumption. Because control frames are short, between 200 and about 900 bits against 4,000-bit readings, their energy amounts to only 0.6–2.3% of the data-

transmission energy. Charging this overhead to the proposal alone narrows its advantage in energy per delivered bit over the strongest baseline from 21.1–22.1% to 19.3–21.6%; the advantage would disappear only if control traffic cost more than about 27% of the data energy, an order of magnitude above the upper estimate. The comparison is conservative, because the baselines also need control traffic that is not charged here: under the same assumptions, a distributed LEACH-style set-up with advertisement, join and schedule frames in every round would cost of the order of 5-8% of the data energy. The estimate excludes MAC contention, idle listening and synchronisation, which Section 8 treats as threats to validity.

7. DISCUSSION

7.1 What actually drives the gains

Read together, Sections 6.6 and 6.7 support a single conclusion: in this problem the architecture matters and the intelligence is largely decorative. The two mechanisms that survive ablation are structural - how many clusters to form, and how their heads reach the sink - and both are cheap. The fuzzy layer and the metaheuristic, which occupy most of the design effort in this literature, contribute a small and scenario-dependent residue. We do not claim this generalises to every fuzzy-metaheuristic aggregation scheme; we do claim that it is the kind of result that cannot be excluded by any study that omits ablation, and that none of the schemes in Table 1 reports such a test.

7.2 Metric pitfalls

Three metric choices would each have reversed a conclusion in this study. LND alone would rank LEACH first in Scenario C, where it is plainly worst. Mean residual energy would rank EEO above the proposal in all three scenarios, because a protocol that transmits less retains more. Jain's index over residual energy would do the same: EEO attains 0.910 in Scenario C against 0.832 for the proposal, since perfect balance is trivially achieved by a protocol that does little work. Energy per delivered bit is immune to all three inversions because it is normalised by delivered payload, and we recommend it as the primary figure of merit.

7.3 Relation to the closest antecedent

FCEO [8] reports that fuzzy-controlled EO outperforms LEACH, Fuzzy-LEACH and EEO on alive nodes, residual energy and PDR. In our reproduction under an explicit link model, FCEO is the weakest of the five protocols on energy per delivered bit in Scenarios A and B (0.1794 and 0.2556 µJ/bit) and has the lowest HND in both, and it degrades with density. Two differences explain this. Its fixed gateway layer concentrates traffic on a quarter of the heads regardless of their energy state, and its evaluation charges no energy for retransmissions, so the cost of forwarding an aggregate over a marginal link is invisible to its fitness function. This is not evidence that the original results were computed incorrectly; it is evidence that they were computed under assumptions that remove the phenomenon their mechanism was designed to address.

7.4 Role in automated network operation

From the standpoint of automated systems, UA-IT2F/AEO is a two-rate supervisory control loop over the network. Its measured state is the vector of residual energies together with the link statistics rel, v and n, updated in every round (Algorithm 1, line 16); its decision variables are the CH schedule and the forwarding parents; and its controlled outputs are energy per delivered bit, delivery ratio and the timing of node deaths. The slow loop, executed every Tc rounds or on a CH failure, solves a multi-objective assignment problem whose weights encode the operator's priorities (Section 4.4). The fast loop, executed every round, re-solves only the backbone from fresh energy and reliability feedback. The ablation of Section 6.7 shows where the regulation actually happens: in a feedback-driven set-point for the number of heads, Eq. (23), recomputed from the surviving node count, and in the fast routing loop, which reacts to the state of each relay before it is exhausted. The estimation and search layers refine decisions that these two mechanisms have already largely determined.

As an operational example, consider condition monitoring in a production hall of about 100 m × 100 m, in which 100 battery-powered nodes on motors, pumps and conveyors report vibration and temperature once per reporting period to a gateway in an adjoining control room outside the monitored area - the geometry of Scenario C [15]. Metal structures and moving equipment produce shadowing that persists over many periods, which is the situation modelled by Eqs. (5) and (6), and the maintenance system that consumes the data needs a predictable delivery ratio rather than a long survival of a few nodes. The procedure would then run at the gateway. At commissioning it collects node positions and initial link statistics and forms the first clustering; in every period it updates the backbone from the energy fields carried by the incoming aggregates; when a head fails or T_c periods have elapsed it re-clusters; and it can alert the operator when the adaptive count reaches the lower bound of its band or the delivery ratio falls below a set threshold, both of which indicate that the network needs maintenance. Section 6.9 indicates that the control traffic of this loop is small compared with the data traffic, and Section 7.1 that the loop can be simplified without measurable loss by omitting the type-2 and adaptive-controller layers where gateway computation or configuration effort matters.

8. THREATS TO VALIDITY

Simulation only. All results come from a discrete-round simulator written for this study; no physical testbed measurements are reported. Absolute values therefore depend on the model, and only relative comparisons under identical accounting should be taken as evidence. The twenty deployments per scenario support the paired statistics reported, but they share one channel and energy model and therefore sample variability of topology and channel realisation, not of the model itself.

Channel abstraction. Shadowing is modelled per node rather than per link to keep the per-round cost linear, interference and MAC contention are not modelled, and the BER expression assumes coherent detection; ARQ attempts are therefore assumed collision-free. A protocol that concentrates traffic on few relays, as ours does, would face more contention in reality

than the model charges it.

Control overhead. The simulated results charge no energy for disseminating clustering and routing decisions, for the proposal or for the baselines. Section 6.9 estimates this overhead analytically at 0.6-2.3% of the data energy, which narrows the energy advantage over the strongest baseline from 21.1-22.1% to 19.3-21.6%. The estimate assumes a centralised implementation, collision-free control frames and no idle listening, and has to be confirmed by MAC-level simulation or on a testbed.

Cluster-size imbalance. Cost-based member assignment occasionally produces one very large cluster, visible in Scenario C in Figure 2. The fitness penalises the energy consequence but not the size directly, and an explicit balance constraint would likely improve early-death behaviour. Section 4.1 explains how the imbalance arises from the small adaptive count, the attraction of heads to the sink-side edge and the endpoint structure of the shadowing model.

Scope of the null results. The absence of a measurable type-2 benefit is established for this rule base, this footprint parameterisation and these scenarios. It is evidence against the mechanism being load-bearing here, not proof that type-2 inference cannot help in other formulations.

9. CONCLUSIONS

This paper proposed UA-IT2F/AEO, a multi-scale data aggregation framework for WSNs, and evaluated it under a link model in which frames are lost and retransmissions cost energy. Across three scenarios it reduced energy per delivered bit by 21.1-22.1% relative to the strongest baseline and raised the delivery ratio, with all paired comparisons significant after correction.

A component-level ablation showed that these gains originate in two structural mechanisms, the adaptive cluster count and the energy- and reliability-aware multi-hop backbone refreshed every round, with the fairness and rotation terms protecting against early node death. The interval type-2 layer and the uncertainty-aware optimizer controller produced no statistically significant network-level effect under the tested conditions, which Sections 4.4 and 6.6 attribute to the small weight of the fuzzy score in the fitness and to the small share of the improvement contributed by iterative refinement. For automated operation this means that the essential loop is simple: a feedback-driven set-point for the number of heads and a per-round routing update.

These conclusions are bounded by the adopted simulation model. They rest on twenty simulated deployments per scenario, without MAC contention, idle listening or synchronisation, and with control-message energy estimated analytically rather than simulated; that estimate narrows the advantage but does not remove it, and a full accounting at the MAC level could narrow it further. Absolute values should therefore not be transferred to a deployment, and only the relative ordering under identical accounting is supported. Future work will address these limits directly through a low-overhead implementation that piggybacks state on data frames and issues routing updates only when the energy ranking of the relays changes, an explicit cluster-balance constraint, MAC-level simulation, and validation of the relative ordering on a physical network such as an industrial monitoring testbed. More generally, we recommend that evaluations of aggregation protocols model frame loss and charge retransmission energy, and that reported gains be attributed by ablation against an otherwise identical architecture before being credited to a fuzzy or metaheuristic component.

Reproducibility. The complete simulator, experiment driver, analysis scripts and figure generation code accompany this manuscript. All reported figures and tables are produced end to end from that code with fixed seeds.

REFERENCES

[1] Heinzelman, W.R., Chandrakasan, A., Balakrishnan, H. (2000). Energy-efficient communication protocol for wireless microsensor networks. In Proceedings of the 33rd Annual Hawaii International Conference on System Sciences, Maui, HI, USA, p. 10. https://doi.org/10.1109/HICSS.2000.926982

[2] Heinzelman, W.B., Chandrakasan, A.P., Balakrishnan, H. (2002). An application-specific protocol architecture for wireless microsensor networks. IEEE Transactions on Wireless Communications, 1(4): 660-670. https://doi.org/10.1109/TWC.2002.804190

[3] Lindsey, S., Raghavendra, C.S. (2002). PEGASIS: Power-efficient gathering in sensor information systems. In Proceedings, IEEE Aerospace Conference, Big Sky, MT, USA, p. 3. https://doi.org/10.1109/AERO.2002.1035242

[4] Younis, O., Fahmy, S. (2004). HEED: A hybrid, energy-efficient, distributed clustering approach for ad hoc sensor networks. IEEE Transactions on Mobile Computing, 3(4): 366-379. https://doi.org/10.1109/TMC.2004.41

[5] Del-Valle-Soto, C., Rodríguez, A., Ascencio-Piña, C.R. (2023). A survey of energy-efficient clustering routing protocols for wireless sensor networks based on metaheuristic approaches. Artificial Intelligence Review, 56(9): 9699-9770. https://doi.org/10.1007/s10462-023-10402-w

[6] Mezher, M.A., Din, S., Ilyas, M., Bayat, O., Abbasi, Q. H., Ashraf, I. (2024). Data transmission enhancement using optimal coding technique over in vivo channel for interbody communication. Big Data, 12(6): 556-568. https://doi.org/10.1089/big.2021.0224

[7] Phoemphon, S., So-In, C., Aimtongkham, P., Nguyen, T.G. (2021). An energy-efficient fuzzy-based scheme for unequal multihop clustering in wireless sensor networks. Journal of Ambient Intelligence and Humanized Computing, 12(1): 873-895. https://doi.org/10.1007/s12652-020-02090-z

[8] Idan, Z.S., Al-Khazaali, A.A.T., Alaasam, H.A.H., Alrammahi, H., Al-Mayali, Y.M.H. (2026). A fuzzy-controlled equilibrium optimizer for energy-efficient and reliable multi-level data aggregation in wireless sensor networks. Journal Européen des Systèmes Automatisés, 59(7): 1857-1865. https://doi.org/10.18280/jesa.590704

[9] Zadeh, L.A. (1975). The concept of a linguistic variable and its application to approximate reasoning—I. Information Sciences, 8(3): 199-249. https://doi.org/10.1016/0020-0255(75)90036-5

[10] Mamdani, E.H. (1974). Application of fuzzy algorithms for control of simple dynamic plant. Proceedings of the Institution of Electrical Engineers, 121(12): 1585-1588. https://doi.org/10.1049/piee.1974.0328

[11] Faramarzi, A., Heidarinejad, M., Stephens, B., Mirjalili, S. (2020). Equilibrium optimizer: A novel optimization algorithm. Knowledge-Based Systems, 191: 105190. https://doi.org/10.1016/j.knosys.2019.105190
[12] Wolpert, D.H., Macready, W.G. (1997). No free lunch theorems for optimization. IEEE Transactions on Evolutionary Computation, 1(1): 67-82. https://doi.org/10.1109/4235.585893
[13] Sörensen, K. (2015). Metaheuristics—The metaphor exposed. International Transactions in Operational Research, 22(1): 3-18. https://doi.org/10.1111/itor.12001
[14] Camacho-Villalón, C.L., Dorigo, M., Stützle, T. (2023). Exposing the grey wolf, moth-flame, whale, firefly, bat, and antlion algorithms: Six misleading optimization techniques inspired by bestial metaphors. International Transactions in Operational Research, 30(6): 2945-2971. https://doi.org/10.1111/itor.13176
[15] Gungor, V.C., Hancke, G.P. (2009). Industrial wireless sensor networks: Challenges, design principles, and technical approaches. IEEE Transactions on Industrial Electronics, 56(10): 4258-4265. https://doi.org/10.1109/TIE.2009.2015754
[16] Vuran, M.C., Akan, Ö.B., Akyildiz, I.F. (2004). Spatio-temporal correlation: Theory and applications for wireless sensor networks. Computer Networks, 45(3): 245-259. https://doi.org/10.1016/j.comnet.2004.03.007
[17] Mendel, J.M., John, R.B. (2002). Type-2 fuzzy sets made simple. IEEE Transactions on Fuzzy Systems, 10(2): 117-127. https://doi.org/10.1109/91.995115
[18] Karnik, N.N., Mendel, J.M. (2001). Centroid of a type-2 fuzzy set. Information Sciences, 132(1-4): 195-220. https://doi.org/10.1016/S0020-0255(01)00069-X
[19] Nie, M., Tan, W.W. (2008). Towards an efficient type-reduction method for interval type-2 fuzzy logic systems. In 2008 IEEE International Conference on Fuzzy Systems (IEEE World Congress on Computational Intelligence), Hong Kong, China, pp. 1425-1432. https://doi.org/10.1109/FUZZY.2008.4630559
[20] Wu, D., Mendel, J.M. (2007). Uncertainty measures for interval type-2 fuzzy sets. Information Sciences, 177(23): 5378-5393. https://doi.org/10.1016/j.ins.2007.07.012
[21] Rawat, P., Chauhan, S. (2021). Clustering protocols in wireless sensor network: A survey, classification, issues, and future directions. Computer Science Review, 40: 100396. https://doi.org/10.1016/j.cosrev.2021.100396
[22] El Khediri, S. (2022). Wireless sensor networks: A survey, categorization, main issues, and future orientations for clustering protocols. Computing, 104(8): 1775-1837. https://doi.org/10.1007/s00607-022-01071-8
[23] El Khediri, S., Selmi, A., Khan, R.U., Moulahi, T., Lorenz, P. (2024). Energy efficient cluster routing protocol for wireless sensor networks using hybrid metaheuristic approache's. Ad Hoc Networks, 158: 103473. https://doi.org/10.1016/j.adhoc.2024.103473
[24] Rao, C., Kan, M., Zhou, P., Lan, Y. (2025). A novel multi objective energy efficient clustering optimization scheme based on heuristic intelligence for wireless sensor networks. Scientific Reports, 15(1): 36988. https://doi.org/10.1038/s41598-025-21918-2
[25] Zhang, S., Liu, X., Trik, M. (2025). Energy efficient multi hop clustering using artificial bee colony metaheuristic in WSN. Scientific Reports, 15(1): 26803. https://doi.org/10.1038/s41598-025-11318-x
[26] Liu, Y., Ding, H., Wang, Z., Dhiman, G., Yang, Z., Hu, P. (2023). An enhanced equilibrium optimizer for solving optimization tasks. Computers, Materials and Continua, 77(2): 2385-2406. https://doi.org/10.32604/cmc.2023.039883
[27] Al-Betar, M.A., Abu Doush, I., Makhadmeh, S.N., Al-Naymat, G., Alomari, O.A., Awadallah, M.A. (2024). Equilibrium optimizer: A comprehensive survey. Multimedia Tools and Applications, 83(10): 29617-29666. https://doi.org/10.1007/s11042-023-16764-1
[28] Naghibi, M., Barati, H. (2021). SHSDA: Secure hybrid structure data aggregation method in wireless sensor networks. Journal of Ambient Intelligence and Humanized Computing, 12(12): 10769-10788. https://doi.org/10.1007/s12652-020-02751-z
[29] Saeedi, I.D.I., Al-Qurabat, A.K.M. (2022). Perceptually important points-based data aggregation method for wireless sensor networks. Baghdad Science Journal, 19(4): 13. https://doi.org/10.21123/bsj.2022.19.4.0875
[30] Hajian, R., Erfani, S.H. (2021). CHESDA: Continuous hybrid and energy-efficient secure data aggregation for WSN. The Journal of Supercomputing, 77(5): 5045-5075. https://doi.org/10.1007/s11227-020-03455-z
[31] Bharathi, S.D., Veni, S. (2025). Geographical energy-aware data aggregation using mobile sinks (GEADAMS) algorithm in wireless sensor networks to minimize latency. International Journal of Performability Engineering, 21(5): 288-297. https://doi.org/10.23940/ijpe.25.05.p6.288297
[32] Kaur, A., Bansal, M., Kumar, D. (2025). Mobile agent and ACO based data aggregation for wireless sensor network. SN Computer Science, 6(1): 77. https://doi.org/10.1007/s42979-024-03583-w
[33] Dhanaraj, R.K., Lalitha, K., Anitha, S., Khaitan, S., Gupta, P., Goyal, M.K. (2021). Hybrid and dynamic clustering based data aggregation and routing for wireless sensor networks. Journal of Intelligent & Fuzzy Systems, 40(6): 10751-10765. https://doi.org/10.3233/JIFS-201756
[34] Yousefpoor, E., Barati, H., Barati, A. (2021). A hierarchical secure data aggregation method using the dragonfly algorithm in wireless sensor networks. Peer-to-Peer Networking and Applications, 14(4): 1917-1942. https://doi.org/10.1007/s12083-021-01116-3
[35] Yun, W.K., Yoo, S.J. (2021). Q-learning-based data-aggregation-aware energy-efficient routing protocol for wireless sensor networks. IEEE Access, 9: 10737-10750. https://doi.org/10.1109/ACCESS.2021.3051360
[36] Bhushan, S., Kumar, M., Kumar, P., Stephan, T., Shankar, A., Liu, P. (2021). FAJIT: A fuzzy-based data aggregation technique for energy efficiency in wireless sensor network. Complex & Intelligent Systems, 7(2): 997-1007. https://doi.org/10.1007/s40747-020-00258-w
[37] Sharmin, S., Ahmedy, I., Md Noor, R. (2023). An energy-efficient data aggregation clustering algorithm for wireless sensor networks using hybrid PSO. Energies, 16(5): 2487. https://doi.org/10.3390/en16052487
[38] Zuniga, M., Krishnamachari, B. (2004). Analyzing the transitional region in low power wireless links. In 2004 First Annual IEEE Communications Society Conference on Sensor and Ad Hoc Communications and Networks, Santa Clara, CA, USA, pp. 517-526. https://doi.org/10.1109/SAHCN.2004.1381954

[39] Iqbal, S., Ahmed, A., Siraj, M., Al Tamimi, M., Bhangwar, A.R., Kumar, P. (2023). A multi-hop QoS-aware and predicting link quality estimation (PLQE) routing protocol for reliable WBSN. IEEE Access, 11: 35993-36003. https://doi.org/10.1109/ACCESS.2023.3266067

[40] Hu, H. (2024). Impacts of transmission power control on link quality estimation in wireless sensor networks. IEEE Access, 12: 61388-61400. https://doi.org/10.1109/ACCESS.2024.3368381

[41] Tao, Y., Zhang, J., Yang, L. (2020). An unequal clustering algorithm for wireless sensor networks based on interval type-2 TSK fuzzy logic theory. IEEE Access, 8: 197173-197183. https://doi.org/10.1109/ACCESS.2020.3034607

[42] Al-Hussain, E.A., Al-Suhail, G.A. (2025). Energy-aware clustering using intelligent scheme for heterogeneous wireless sensor networks. Karbala International Journal of Modern Science, 11(2): 3. https://doi.org/10.33640/2405-609X.3400

[43] Jain, R.K., Chiu, D.M.W., Hawe, W.R. (1984). A quantitative measure of fairness and discrimination. Eastern Research Laboratory, Digital Equipment Corporation, Hudson, MA.

[44] Demšar, J. (2006). Statistical comparisons of classifiers over multiple data sets. Journal of Machine Learning Research, 7: 1-30.

[45] Wilcoxon, F. (1945). Individual comparisons by ranking methods. Biometrics Bulletin, 1(6): 80-83. https://doi.org/10.2307/3001968

[46] Holm, S. (1979). A simple sequentially rejective multiple test procedure. Scandinavian Journal of Statistics, 6(2): 65-70.

[47] Cliff, N. (1993). Dominance statistics: Ordinal analyses to answer ordinal questions. Psychological Bulletin, 114(3): 494-509. https://doi.org/10.1037/0033-2909.114.3.494

[48] IEEE. (2020). IEEE Standard for Low-Rate Wireless Networks. IEEE Std 802.15.4-2020. IEEE, New York, USA. https://doi.org/10.1109/IEEESTD.2020.9144691

NOMENCLATURE

a_1	exploration gain of the Equilibrium Optimizer, dimensionless
ASS	aggregation suitability score, dimensionless
b	size of an aggregate emitted by a cluster head, bit
d	distance between two nodes, m
d_0	crossover distance of the radio model, m
$\hat{D}$	normalised distance to the sink, dimensionless
E	residual energy of a node, J
E_0	initial energy of a node, J
E_{DA}	aggregation energy per bit, J.bit^{-1}
E_{elec}	energy of the radio electronics per bit, J.bit^{-1}
E_{rx}, E_{tx}	energy to receive and to transmit a frame, J
GP	generation probability of the Equilibrium Optimizer, dimensionless
J	Jain's fairness index, dimensionless
k	length of a reading, bit
k_{opt}	adaptive number of cluster heads, dimensionless
m	number of cluster heads, dimensionless
M	side length of the deployment field, m
n	path-loss exponent, dimensionless
N	number of deployed sensor nodes, dimensionless
N_a	number of alive nodes, dimensionless
P_n	noise floor, dBm
P_t	transmit power, dBm
P^s	success probability of a hop under ARQ, dimensionless
PL	path loss, dB
R	maximum number of ARQ attempts, dimensionless
T_c	re-clustering period, rounds
u	per-node uncertainty index, dimensionless
U	network uncertainty index, dimensionless
v	exponentially weighted dispersion of the observed PRR, dimensionless
X	log-normal shadowing term, dB

Greek symbols

β	forgetting factor of the exponential weighting, dimensionless
γ	signal-to-noise ratio, dB
Δ	half-width of the footprint of uncertainty, dimensionless
ε_{fs}	free-space amplifier energy, J.bit^{-1}.m^{-2}
ε_{mp}	multipath amplifier energy, J.bit^{-1}.m^{-4}
η	energy per delivered bit, J.bit^{-1}
θ	correlation length of the readings, m
π	packet reception ratio of a link, dimensionless
ρ	correlation coefficient of the shadowing process, dimensionless
σ	standard deviation of shadowing, dB
Φ	fitness of a candidate solution, dimensionless
ψ	control variable of the adaptive optimizer, dimensionless

Subscripts

a	alive
c, c'	cluster heads
i, j	node indices
l, u	lower and upper bounds of an interval type-2 set
q	rule index